

TRANSPORT OF ACCELERATOR PRODUCED NEUTRONS IN A CONCRETE ROOM

R. C. McCall, T. M. Jenkins and R. A. Shore*

Stanford Linear Accelerator Center, Stanford, CA 94305

ABSTRACT

The production of photoneutrons by electron accelerators is an unavoidable process at operating energies above about 10 MeV. These photoneutrons create problems in shielding, personnel protection, and induced radioactivity. This paper attempts to describe the neutron field spectral and intensity distributions. The initial spectrum and modifying effects of photon shielding materials and concrete room shielding are considered. The relative yields of neutrons and photons as a function of the primary electron energy are described. Both experimental and Monte Carlo results are presented. It is shown that the average energy of the neutron spectrum is a useful parameter for shielding calculations, fluence-to-dose equivalent conversions, and spectral degradation calculations.

INTRODUCTION

In electron accelerators operating above about 10 MeV there is an unavoidable contamination of photoneutrons produced. These have been of concern to various authors and to regulatory authorities for their effects on the patient in medical accelerators. The magnitude of the photoneutron contamination problem is not well understood. Neutrons are difficult to measure in such an environment since there is the problem of measuring the neutrons in the presence of high-intensity and high-energy photons. Most neutron detectors respond to these photons^{1,2,3}. In addition, the photoneutron spectrum is not well-known which makes interpretation of measurements in terms of dose equivalent almost impossible. Although the primary photo-neutron spectrum may be known, the effect of the photon shielding around the target assembly on the neutron spectrum is not well-understood and the accelerators are almost always in a shielded concrete room which produces a further complication due to wall scattering. As a result, the measurements which have been reported often suffer from one or more of the following problems;

1. There is an unsuspected response of the neutron detectors to high-energy photons and as a result, the reported neutron measurements have been too high.
2. The experimenter has used a detector which measures fluence and has made incorrect assumptions regarding the spectrum of the neutrons being measured and hence the efficiency of the detector.
3. The experimenter has used a detector measuring dose equivalent and has made similar incorrect assumptions resulting in similar errors as in 2 above.

4. The experimenter has measured fluence and then performed calculations to convert this fluence into dose equivalent. An incorrect assumption of the spectrum of the neutrons being measured will cause an error in the calculated dose equivalent.
5. The experimenter has measured fluence or dose equivalent at some point distant from the machine and assumed an inverse square relationship. In the high-scattering geometry of a concrete room this assumption is invalid.

It is the purpose of this paper to explore some of these problems experimentally and theoretically and find a better solution to this measurement problem.

NEUTRON PRODUCTION

In electron accelerators, neutrons are produced almost entirely by high-energy photons. Direct production of neutrons by electrons is more than two orders of magnitude smaller and can be neglected. For electron energies below about 50 MeV, the production is almost entirely from the giant photonuclear resonance, commonly called just the giant resonance. This term refers to the prominent, rather broad, peak in the photoneutron cross section curves at 13-18 MeV for heavy and medium nuclei. For lighter nuclei ($A < 40$), the peak is at somewhat higher energies.

The giant resonance process produces two groups of neutrons. The first and largest has a spectrum which can be described by a Maxwellian distribution as follows.

$$\frac{dN}{dE_n} = \frac{E_n}{T} e^{-\frac{E_n}{T}}$$

where T is the nuclear temperature in MeV. For materials of interest, the nuclear temperature typically lies between 0.4 and 1.0 MeV although it is a mild function of the exciting energy. It should be noticed that the most probable energy (the peak of the spectrum) is at $E_n = T$ and the average energy is at $E_n = 2T$. The second group of neutrons are produced by direct emission and are somewhat higher in energy. This group amounts to 10-20% of the total neutrons in general.

Figure 1⁴, shows some typical spectra of photoneutrons. The direct process neutrons appear as a bump on the high-energy side. A similar comparison, with a lower energy photoneutron spectrum is shown in Figure 2 with a fission spectrum superimposed⁵. The similarity is quite marked.

A good review of photoneutron production as well as an extensive list of older references is given by Swanson^{6,7,8}. Figure 3 is taken from Swanson⁸ and shows the neutron yield per kilowatt of electrons incident on thick targets of various elements.

*Work supported by the Department of Energy under Contract EY 76-C-03-0515.

EFFECTS OF ACCELERATOR HEAD SHIELDING

The spectra described in the previous section are what would be obtained from relatively thin targets struck by electrons or a bremsstrahlung beam. A typical accelerator has massive shielding around the target to provide photon shielding and produce a collimated beam of x-rays. Unlike bremsstrahlung, the neutrons are produced approximately isotropically and penetrate the head shielding in all directions. The photon shielding is commonly of some heavy metal such as tungsten, lead or iron, and the only significant neutron energy-loss mechanisms in these materials are either inelastic scattering, (n,n',γ) , or $(n,2n)$ reactions. In general, both of these processes are effective in the MeV energy region while the $(n,2n)$ reaction is most effective at the higher energies. Inelastic scattering can occur only at energies above the lowest excited state of the shielding material. These lowest excited states are listed for the isotopes of iron, lead and tungsten in Table 1. The amount of energy loss in any inelastic collision cannot be exactly determined, but there is a minimum energy loss equal to the energy of the lowest excited state, and there is often a cascade of gammas following excitation of much higher energy states such that there is a considerable energy loss per collision. In the $(n,2n)$ reaction, there is a minimum energy loss equal to the binding energy of a neutron. The two emerging neutrons tend to be of similar energy and produce large numbers of quite low energy neutrons. Since the total of the inelastic plus $(n,2n)$ cross sections is of the order of 1 or 2 barns for these materials, there are several collisions produced for the typical neutron penetrating the photon shielding. Thus, any anisotropy in the initial angular distribution of the photon neutrons has been destroyed by the time the neutrons reach the outside of the head shielding. There is, in addition, a large amount of elastic scattering taking place at these energies in these materials. This produces no energy loss but does however have the effect of producing a longer path length for the neutrons in the shielding material and offering a greater opportunity for the inelastic and the $(n,2n)$ reactions to occur. There is very little attenuation of neutrons since the capture cross sections of these materials are very small, at least down to thermal energies. If one were to measure attenuation in these materials, extremely long half-value layers would be observed. With a spectrum containing high-energy neutrons such as a fission spectrum or a plutonium beryllium spectrum, there can, in fact, be a slight buildup of neutrons due to the $(n,2n)$ reactions.

EFFECTS OF THE CONCRETE ROOM

Most accelerators are in a shielded room, most commonly made of concrete. Neutrons striking the concrete undergo mostly elastic scattering. The hydrogen in the concrete thermalizes the neutrons fairly rapidly and they are then captured, usually with accompanying gamma-ray emission. Many of the neutrons may scatter back out of the walls and traverse the room several times before capture. The result is a low-energy scattered component of the neutron spectrum everywhere in the room. Patterson and Wallace⁹ showed that with a fast neutron source in a cavity in concrete, the thermal fluence is approximately constant throughout the room. Since this point on the scattered spectrum is constant throughout the room, it is reasonable to assume that the entire scattered spectrum is constant. This assumption will be examined in a later section of this paper. At any point in the room, then, the neutron spectrum will consist of a constant component plus a

component varying as the inverse square of the distance to the accelerator head.

CALCULATIONS

It is impractical to make analytical calculations of the effects of neutron scattering in anything but the simplest geometry. Measurements of the spectra would be extremely difficult and time consuming. In order to examine these problems, we have used the Monte Carlo neutron-transport code, MORSE, from Oak Ridge¹⁰. MORSE is a multipurpose neutron and gamma-ray transport Monte Carlo code where the solution of neutron, gamma-ray, or coupled neutron, gamma-ray problems may be obtained in either the forward or the adjoint mode. General three-dimensional geometry may be used with an albedo option at any material surface. It will be shown that MORSE provides a suitably accurate prediction of the effects of neutron scattering in complex geometries, so that we can use it to evaluate the neutron fields around a small accelerator.

Several tests of MORSE were made. In the first, we have made some comparisons of MORSE calculations with some experiments utilizing a ^{252}Cf fission neutron source. In order to minimize the effects of scattering, the measurements were made in a tower made of aluminum struts. The source with an intensity of 2.59×10^8 neutrons/sec, was placed in the tower eleven feet above the ground in an open area well away from buildings. The detectors were placed 6 1/2 feet above the source and the source-detector distance and the height above the ground were kept constant. Lead and iron shields were built up around the source in 2 inch increments using standard 2" by 4" by 8" bricks. The shield was thus approximately a hollow cube with equal thickness on all six sides.

Three detectors were used. A moderated BF_3 counter with a cylindrical polyethylene shield 6 centimeters thick and cadmium outer cover measured fluence, approximately independent of energy. An Andersson-Braun¹¹ detector with a scaler read-out measured dose equivalent, approximately independent of energy. A polyethylene-lined argon- CO_2 filled proton-recoil proportional counter measured neutron energy fluence. The combination of this latter data with the moderated BF_3 counter data gave an estimate of the average neutron energy, \bar{E} . All three counters were in place at all times after we determined that they were not disturbing each other.

For each measurement, counting times were long enough that statistical errors were negligible. The major errors then are systematic and consist of the energy responses of the detectors, and for the \bar{E} measurement, the calibration errors of the proton recoil counter and the moderated BF_3 counter. These errors are difficult to determine, but we would estimate them to be less than $\pm 10\%$ for the relative transmission measurements and somewhat greater than $\pm 10\%$ for the average energy measurements.

In Figure 4 we show the relative transmission of dose equivalent in iron and lead. On the same figure we show the dose equivalent transmission as calculated by MORSE. Similarly in Figure 5 we show the transmission of neutron fluence both calculated and measured. In Figure 6, we show measured and calculated values of \bar{E} . The MORSE calculations were made for hollow spherical shields around the source, so the geometry is not precisely the same. In addition, the MORSE input spectrum was a Cf spectrum as taken from the literature. The Cf neutron source was not a bare Californium

source as was used in the reported fission spectrum, but was a practical source doubly-encapsulated in stainless steel, and had considerable scattering material immediately around it which would degrade the neutron spectrum. With these approximations in mind and the systematic errors discussed above, we feel that this is a reasonable agreement between calculation and measurement. It will be noted that the \bar{E} for the bare Californium source we used was measured to be 1.45 MeV, while the MORSE calculation gives 2.15 MeV which would be typical of a small unencapsulated source. This difference we believe is due to the practical neutron source, and to some residual scattering even in the arrangement which we used.

There was not sufficient tungsten available to perform the type of experiment as done for iron and lead. A measurement was made for the geometry shown in Figure 7 using tungsten, with the dose equivalent and the fluence transmission measured by the same instruments as above. The results of these measurements and the MORSE calculations for the same geometry are shown in Figures 8 and 9. Again we feel that the agreement is reasonably good considering the accuracy of the measurements and the approximation of the practical Californium source spectrum for the theoretical Californium fission spectrum.

As a further test of MORSE, we made measurements in a concrete room similar to what would be used as a radiation therapy room. This room is shown in Figure 10. A radioactive neutron source, in this case a $^{239}\text{PuBe}$ source, was placed 5 ft off the floor in the position as shown. Measurements of dose equivalent and fluence using the same detectors as above were made at various positions approaching the west wall of this room as indicated. Calculations were made of the same geometry using MORSE. The results of these measurements and calculations are shown in Figures 11 and 12 for dose equivalent and fluence respectively, and the agreement is very good.

The above comparisons gave us considerable confidence in the MORSE results and we applied them to some accelerator situations. MORSE gives the dose equivalent at a point as well as a fluence spectrum. An auxiliary program gives fluence, average energy, \bar{E} , and absorbed dose. We took several measured spectra from the literature and put them in our library. In addition to the $^{239}\text{PuBe}$ and ^{252}Cf spectra already measured, we have the following spectra in our library:

<u>Spectrum</u>	<u>Designation</u>
Photoneutrons from 15 MeV electrons on tungsten	15 MeVWPN
Photoneutrons from 25 MeV electrons on Pb	25 MeVPbPN
Photoneutrons from 25 MeV electrons on W	25 MeVWPN

The 15 MeVWPN spectrum was taken from Mutchler⁵. The 25 MeVPbPN spectrum was taken from Breuer¹² and the 25 MeVWPN spectrum was made by an amalgamation of the two spectra from tantalum by Cortini et al⁴. The difference between Ta and W should be slight. It is also possible to use monoenergetic neutrons as the input spectrum.

We first investigated the effects of heavy metal shields on these neutron spectra using MORSE. We used a simple geometry with the source and detector 1 meter apart in vacuum and surrounded the source with spherical shells of the shield material (Pb, Fe or W) to be

studied. The effects on dose equivalent and fluence were found not too much different than in Figures 4 and 5; only tungsten showed significant shielding value. We noted, however, that the effect on \bar{E} is a function of both spectrum and material, as would be expected. Figures 13, 14 and 15 show the effect of shield thickness on the average energy of various neutron spectra for Pb, Fe and W respectively. It can be seen that for each element, the higher energy spectra are degraded more rapidly than lower energy spectra. This is because the nonelastic (inelastic + (n,2n)) cross section increases with energy up to about 2-5 MeV and then stays approximately constant, so that high-energy neutrons are most strongly affected. It is useful to note that \bar{E} decreases exponentially with shield thickness through the range of common head shield thicknesses. Eventually, the curves level out as the energy of most of the neutrons approaches or falls below the first excited state. As expected, W continues to be effective to lower energies than either Pb or Fe. This same exponential decrease of the average energy with shield thickness was found for monoenergetic neutrons and for various neutron spectra with concrete.

We next examined spectra around simulated accelerators and observed the further degradation due to the concrete walls. In the course of these calculations we checked our assumption that the wall scattered neutron contribution was constant around the room. By artificially suppressing the neutrons directly from the source, we calculated only the wall-scattered component at various points in the room shown in Figure 10. In some cases, a direct path shield of tungsten with an artificial density 1000 times normal was imposed. This artificial material (called impervium) gave the same results but was in some ways more versatile. When we ran various sources in this geometry, we observed the following:

1. Scattered fluence was essentially constant for all sources.
2. \bar{E} for the scattered component ranged from about 0.42 MeV for $^{239}\text{PuBe}$ source to about 0.090 MeV for the 15 MeVWPN shielded by 4 inches of W.
3. Scattered fast neutron dose equivalent was greater for the higher-energy spectra, ranging from 2.6×10^{-4} rem/primary neutrons for the 15 MeVWPN spectrum shielded by 4 inches of W to 5.4×10^{-4} rem/primary neutron for $^{239}\text{PuBe}$.

A common assumption in measurements reported in the literature has been that the neutrons measured were close to a fission spectrum. For the primary neutrons, this is a good assumption as shown in Figures 1 and 2. We proceeded to test this assumption in simulated practical conditions, again using MORSE. In Figure 16 we show a comparison of the ^{252}Cf fission spectrum and our 15 MeVWPN spectrum. We have shown an integral spectrum so that one can immediately see what fraction of the neutrons have energies greater than, e.g. that of some threshold detector. In Figure 16 we also show the 15 MeVWPN spectrum filtered with 10 cm of W. Finally, in the same figure, we show the 15 MeVWPN spectrum surrounded by 10 cm thick W shield and placed in the center of the concrete room previously shown. Our detector for this MORSE calculation was one meter from the source. Figure 16 shows clearly that the assumption of a fission spectrum is a poor assumption in a real situation. It also shows the risks in using threshold detectors without good knowledge of the spectrum at the point of measurement.

MEASUREMENTS AND INTERPRETATIONS

In view of the results illustrated in the last section, many of the results reported in the literature must be suspect even when there was no interference from photons. We have developed two methods of measurement of neutron leakage for small accelerators, such as therapy machines, based on our findings. In the first method, we measure fast fluence at various points in the room using moderators and activation foils. We must also measure thermal neutron fluence, e.g. with bare activation foils. The moderator we use¹³ is a cylinder of polyethylene 6 inches diameter by 6 inches long. It is covered with a thermal neutron absorber of either cadmium or boron and a means provided of inserting a gold or indium foil into the center. This detector measures fluence nearly independently of energy. The head shielding and the concrete room is then simulated in MORSE with detectors placed at each of the measurement points. The results of the MORSE calculations are used to provide a conversion factor for converting the measured fluence to absorbed dose or dose equivalent, as desired. We measure the thermal neutron fluence with bare activation foils, convert this to absorbed dose or dose equivalent, and add it to our results. We think this method gives good results but requires lengthy computer calculations for each machine that is measured. Many people wishing to do such measurements do not have access to MORSE or a similar program.

The second method we have developed is of a "cook-book" approach. In the course of performing many MORSE calculations, we have observed a useful fact, illustrated in Figure 17. Here we have plotted the fluence to dose equivalent conversion factor versus average energy, \bar{E} , for many different combinations of input spectra, shielding, concrete room size and position in the room. On the same graph we have plotted the fluence-to-dose equivalent conversion factors for monoenergetic neutrons taken from ICRP Report 21¹⁴. It can be seen that the results fit a straight line nearly parallel to the ICRP monoenergetic values. The dashed line is a least squares fit to the points including many more points than we have actually plotted here. If \bar{E} is known for a measurement point, one can use this graph to convert a fluence measurement to dose equivalent. The average energy, \bar{E} is determined in the following manner. The spectrum at any point in the room is composed of a component coming directly from the accelerator, and a component scattered from the walls. From knowledge of the accelerator energy and shielding, \bar{E} is determined for the direct component from Figures 13-15. In Figure 18, we have plotted the average energy of the room scattered component against the average energy of the source. This did not seem to be a function of room size. It can be seen that for all except the highest energy source (²³⁹PuBe) a linear relationship holds very well. To find \bar{E}_{dir} , the average energy, coming through the head shielding one first determines the average energy of the primary spectrum from the literature. In Figure 19 we have plotted the Half-Energy Layer (HEL) for Pb, Fe, and W as a function of the primary spectrum average energy. From these values we can calculate \bar{E}_{dir} . From a series of MORSE calculations, we found that the fluence of the wall-scattered component is proportional to the inside surface area of the room as found in Ref. 9 for thermal neutrons, i.e.

$$\varphi = \frac{k Q}{S}$$

where Q is the fast-neutron source strength
 S is the inside surface area of the room in cm²
 and k is a constant

From the MORSE runs, we found that k = 4.6 for the W shielded machine and 5.4 for Pb shielded accelerators. The value of k is different since there is no attenuation of the fluence in practical thicknesses of Pb and an attenuation of 0.85 in typical thickness of W.

We can now write the following:

$$\varphi_{tot} = \varphi_{dir} + \varphi_{sc} = \frac{aQ}{4\pi R^2} + \frac{k Q}{S}$$

where the subscripts tot, dir and sc refer to total, direct, and scattered respectively and

a = 1 for Pb shielded machines and 0.85 for W shielded machines

R = distance from accelerator head in cm.

then

$$\bar{E}_{tot} = \frac{a\bar{E}_{dir}}{4\pi R^2} + \frac{k \bar{E}_{sc}}{S}$$

$$\frac{a}{4\pi R^2} + \frac{k}{S}$$

Using the relationship shown in Figure 18, this can be simplified somewhat to

$$\bar{E}_{tot} = \bar{E}_{dir} \left[1 - \frac{0.76k}{aS+k} \frac{4\pi R^2}{4\pi R^2} \right]$$

In making a measurement, all of the factors in this equation are now known and the fast neutron fluence can be converted to D.E. by use of Figure 17. We must convert our measured thermal neutron fluence to D.E. also and add it to the fast neutron D.E. to obtain the total.

In Table II, we list results of calculating the dose equivalent by both methods for several different rooms and accelerators. It can be seen that the agreement is quite good.

TABLE I

Element	Atomic Number	% Abundance	1st Excited State (MeV)
Pb	206	25.1	0.803
	207	21.7	0.570
	208	52.3	2.61
Fe	54	5.8	1.41
	56	91.7	0.847
W	182	26.4	0.100
	183	14.4	0.047
	184	30.6	0.111
	186	28.4	0.123

TABLE II

Dose Equivalent(mrem/rad)

Accelerator Energy	Head Shielding	MORSE Method	Cookbook Method
15	W	0.30	0.29
15	W	0.19	0.18
15	W	0.33	0.31
25	W	2.20	2.23
25	Pb	2.67	2.26

ACKNOWLEDGEMENT

We acknowledge useful discussions regarding photon-neutron source terms with Dr. W. P. Swanson, as well as permission to use Figure 3 prior to its regular publication.

REFERENCES

1. R. C. McCall, T. M. Jenkins and G. D. Oliver, Jr., Med. Phys. 5, 37 (1978).
2. R. C. McCall, T. M. Jenkins and E. Tochilin, "High Energy Photon Response of Moderated Neutron Detectors", Stanford Linear Accelerator Center, Stanford, CA., SLAC-PUB-1718 (1976).
3. A. P. Kushalevsky and G. Shani, Nucl. Inst. Meth. 137, 71 (1976).
4. C. Cortini, C. Milone, A. Ruffino and J. Ferrero as given in NBS Handbook 97, NCRP Report 31, National Committee on Radiation Protection & Measurements (1964).
5. G. S. Mutchler, Ph.D. Dissertation, MIT-2098-224 (1966).
6. W. P. Swanson, Chapt 24 of Radiological Safety Aspects of the Operation of Linear Accelerators, IAEA, Vienna. To be published.
7. W. P. Swanson, "Calculations of Neutron Yields Released by Electrons Incident on Selected Materials", Stanford Linear Accelerator Center, Stanford, CA., SLAC-PUB-2042 (1978), Health Physics 35 353.
8. W. P. Swanson, "Calculation of Neutron Yields Near the Photoneutron Threshold", Stanford Linear Accelerator Center, Stanford, CA., SLAC-PUB-2211, submitted to Health Physics.
9. H. W. Patterson and R. Wallace, "A Method of Calibrating Slow Neutron Detectors", University of California Radiation Laboratory, Berkeley, CA., UCRL-8359 (1958).
10. E. A. Straker, P. N. Stevens, D.C. Irving, and V. R. Cain, "The MORSE Code - A Multigroup Neutron and Gamma Ray Monte Carlo Transport Code", Oak Ridge National Laboratory, ORNL-CFN-70-2-31 (1970).
11. I.O. Anderson and J. Braun, Neutron Dosimetry, Vol 2, 87, IAEA, Vienna (1963).
12. H. Breuer, Z. Naturforsch. 17A, 584 (1962).
13. A. R. Smith, "A Cobalt Neutron-Flux Integrator", University California Radiation Laboratory, Berkeley, CA, UCRL-9212 (1960), and L. D. Stephens and A. R. Smith, "Fast Neutron Survey Using Indium-Foil Activation", UCRL-8418 (1958).
14. International Commission on Radiological Protection (ICRP) Pub 21 (1971).

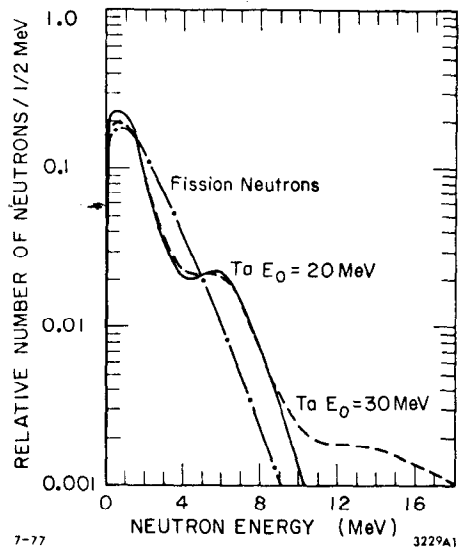


Fig. 1. Typical thick target photoneutron spectra.

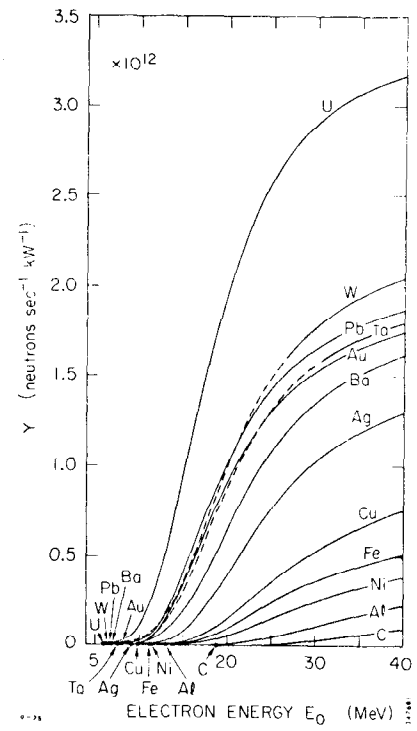


Fig. 3. Thick target neutron yields per kW of electrons incident upon various elements.

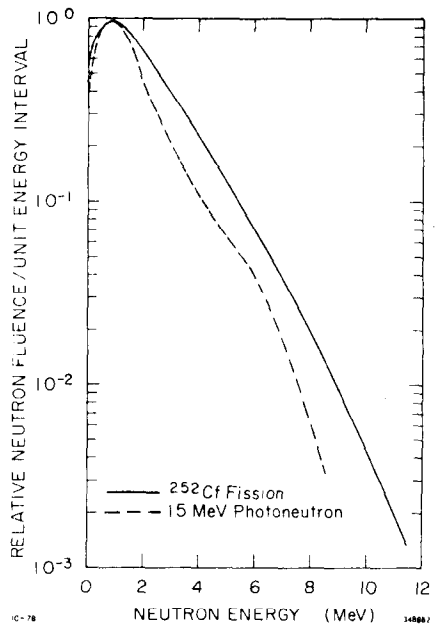


Fig. 2. The photoneutron spectrum from 15 MeV electrons on a thick target compared with ²⁵²Cf fission spectrum.

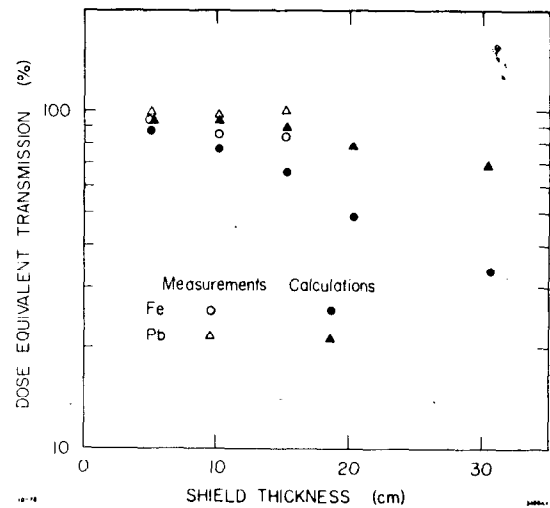


Fig. 4. Measured and calculated relative dose equivalent transmission in Fe and Pb for ²⁵²Cf neutrons.

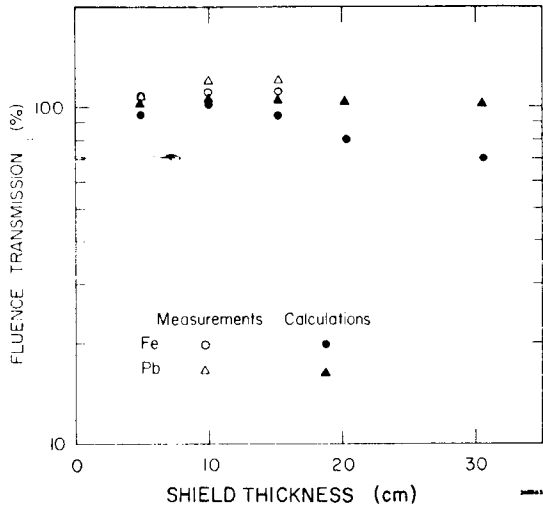


Fig. 5. Measured and calculated relative fluence transmission in Fe and Pb for ^{252}Cf neutrons.

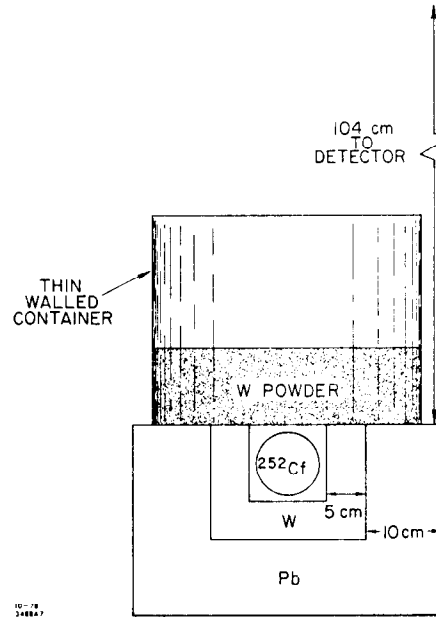


Fig. 7. The geometry used for transmission measurements and calculations in W.

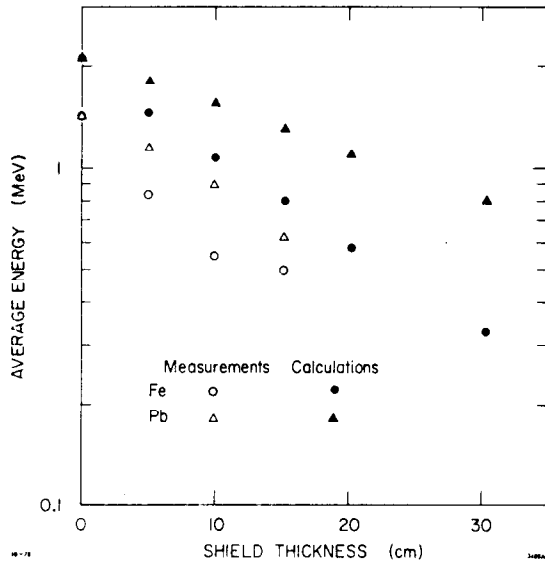


Fig. 6. Measured and calculated values of \bar{E} as a function of thickness in Fe and Pb for ^{252}Cf neutrons.

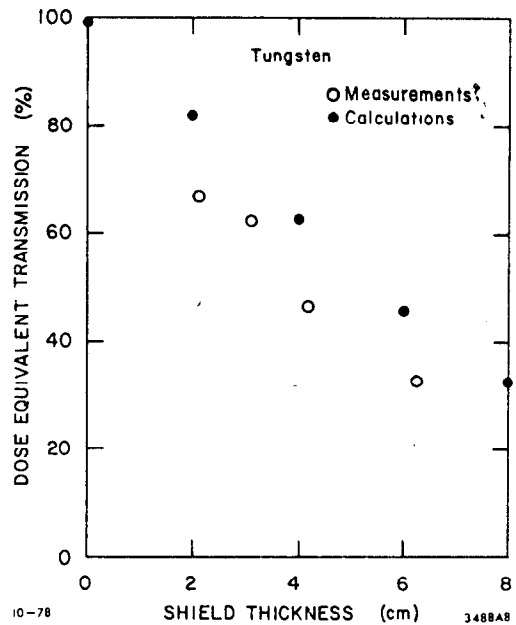


Fig. 8. Measured and calculated relative dose equivalent transmission in W for ^{252}Cf neutrons.

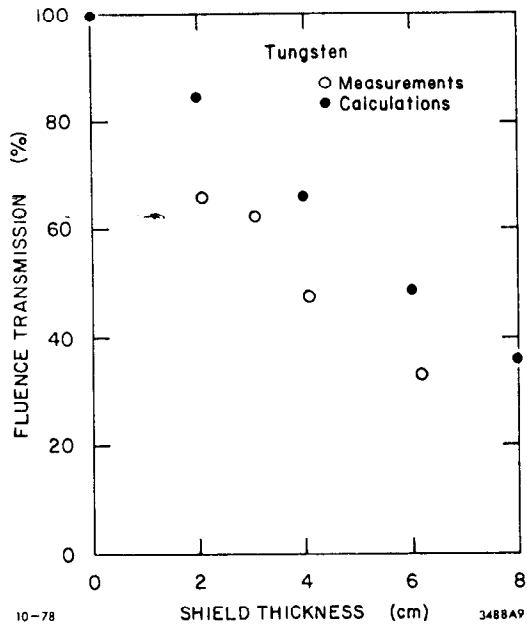


Fig. 9. Measured and calculated relative fluence transmission in W for ^{252}Cf neutrons.

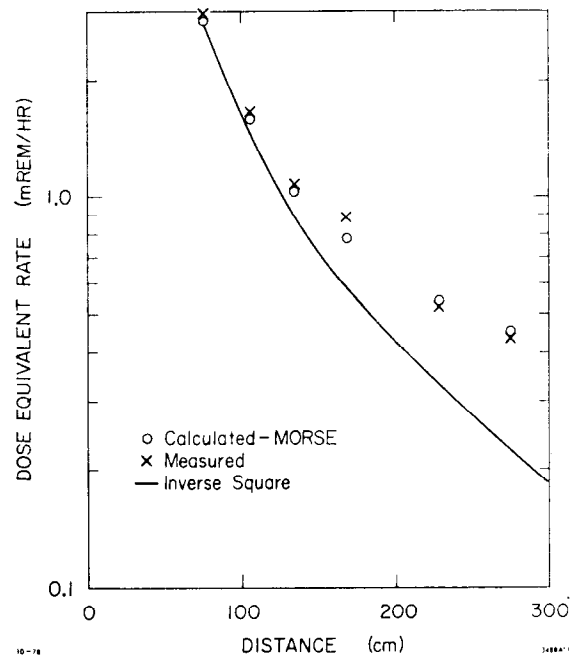


Fig. 11. Measured and calculated dose equivalent rate for a small PuBe source in the geometry of Fig. 10.

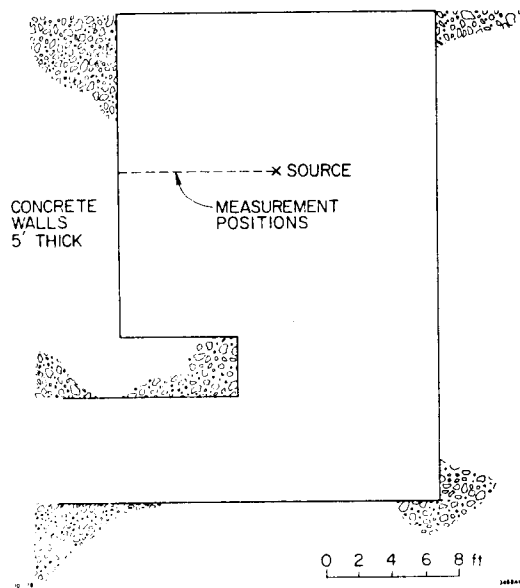


Fig. 10. The shielded room used for measurements and calculations.

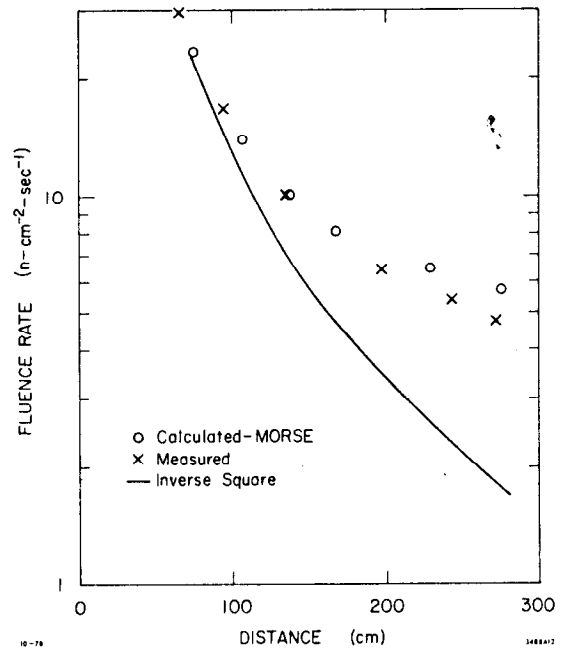


Fig. 12. Measured and calculated fluence rate for a small PuBe source in the geometry of Fig. 10.

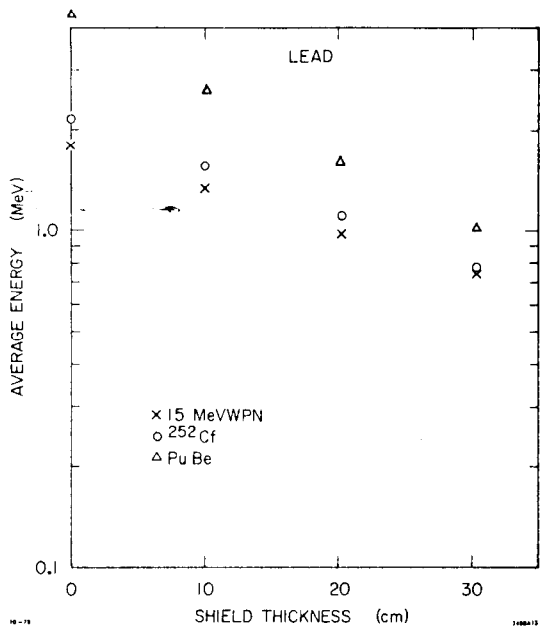


Fig. 13. The calculated average neutron energy as a function of Pb thickness for 15 MeV photoneutron, ²⁵²Cf and PuBe neutron spectra.

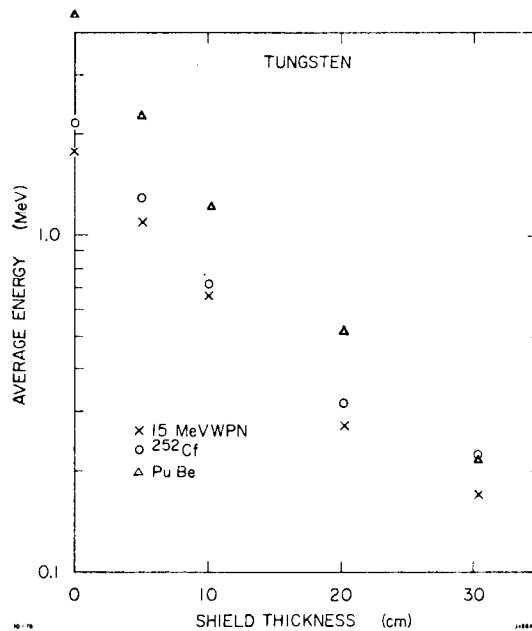


Fig. 15. The calculated average neutron energy as a function of W thickness for 15 MeV photoneutron, ²⁵²Cf and PuBe neutron spectra.

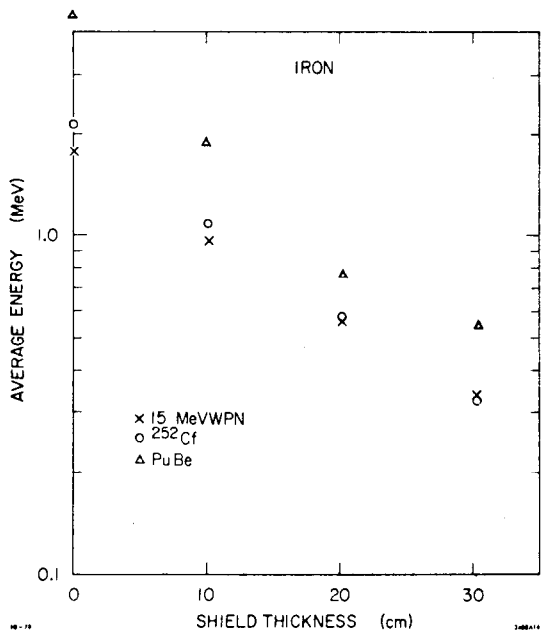


Fig. 14. The calculated average neutron energy as a function of Fe thickness for 15 MeV photoneutron, ²⁵²Cf and PuBe neutron spectra.

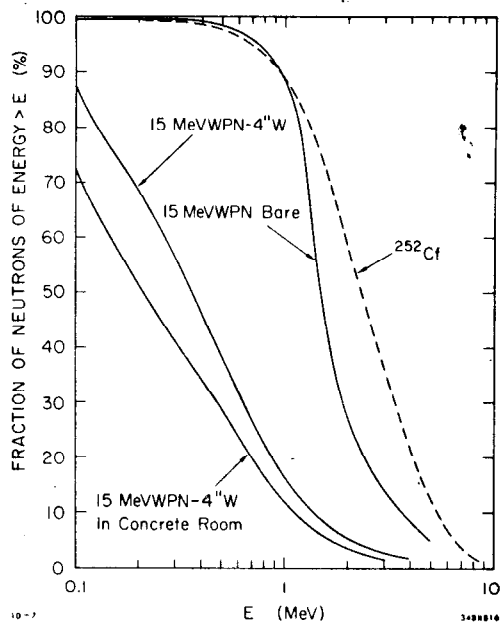


Fig. 16. Comparison of various neutron integral spectra: ²⁵²Cf, 15 MeVWPN-Bare, 15 MeVWPN-4''W, 15 MeVWPN-4''W in a concrete room.

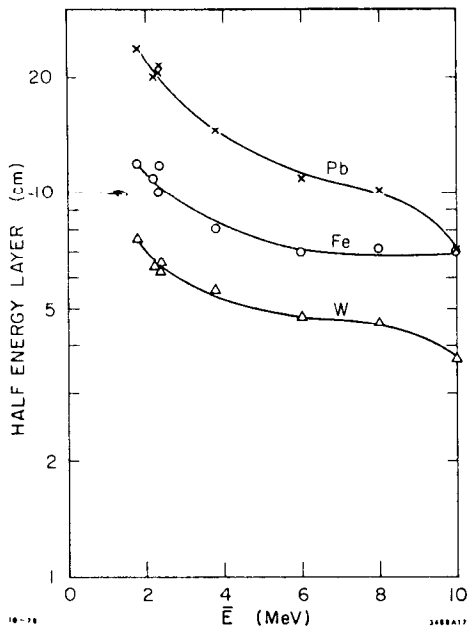


Fig. 17. Fluence-to-Dose equivalent conversion versus average energy and shield geometries. Also the Fluence-to-Dose equivalent conversion for monoenergetic neutrons from ICRP 21.

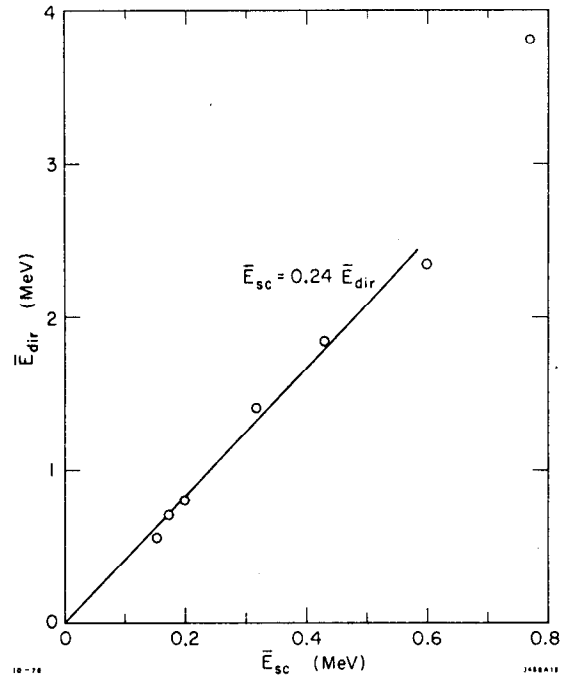


Fig. 18. Average energy of the direct component versus the average energy of the room scattered component for a typical shielded room.

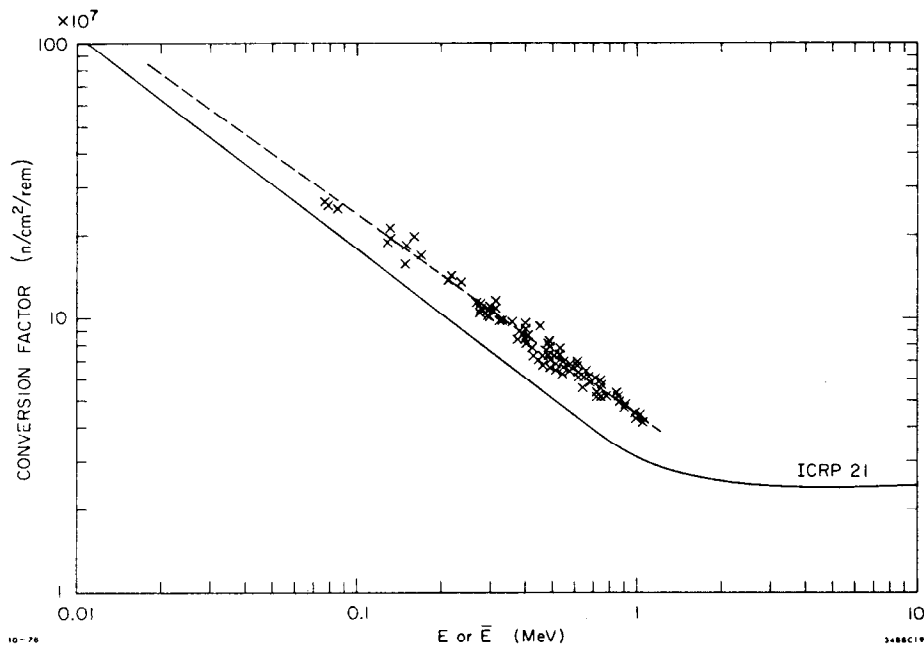


Fig. 19. Half-energy layer (HEL) for Pb, Fe and W as a function of the primary average energy.